

Defect Production By Energetic Particle Bombardment

By

K. L. Merkle

NOTICE

This report was prepared as an account of work sponsored by the United States Government. Neither the United States nor the United States Energy Research and Development Administration, nor any of their employees, nor any of their contractors, subcontractors, or their employees, makes any warranty, express or implied, or assumes any legal liability or responsibility for the accuracy, completeness or usefulness of any information, apparatus, product or process disclosed, or represents that its use would not infringe privately owned rights.

Prepared for Presentation

American Society of Metals, Materials Science Seminar:
 Radiation Damage in Metals
 Cincinnati, Ohio
 November 9-10, 1975

EB



ARGONNE NATIONAL LABORATORY, ARGONNE, ILLINOIS

**operated under contract W-31-109-Eng-38 for the
 U. S. ENERGY RESEARCH AND DEVELOPMENT ADMINISTRATION**

The facilities of Argonne National Laboratory are owned by the United States Government. Under the terms of a contract (W-31-109-Eng-38) between the U. S. Energy Research and Development Administration, Argonne Universities Association and The University of Chicago, the University employs the staff and operates the Laboratory in accordance with policies and programs formulated, approved and reviewed by the Association.

MEMBERS OF ARGONNE UNIVERSITIES ASSOCIATION

The University of Arizona	Kansas State University	The Ohio State University
Carnegie-Mellon University	The University of Kansas	Ohio University
Case Western Reserve University	Loyola University	The Pennsylvania State University
The University of Chicago	Marquette University	Purdue University
University of Cincinnati	Michigan State University	Saint Louis University
Illinois Institute of Technology	The University of Michigan	Southern Illinois University
University of Illinois	University of Minnesota	The University of Texas at Austin
Indiana University	University of Missouri	Washington University
Iowa State University	Northwestern University	Wayne State University
The University of Iowa	University of Notre Dame	The University of Wisconsin

NOTICE

This report was prepared as an account of work sponsored by the United States Government. Neither the United States nor the United States Energy Research and Development Administration, nor any of their employees, nor any of their contractors, subcontractors, or their employees, makes any warranty, express or implied, or assumes any legal liability or responsibility for the accuracy, completeness or usefulness of any information, apparatus, product or process disclosed, or represents that its use would not infringe privately-owned rights. Mention of commercial products, their manufacturers, or their suppliers in this publication does not imply or connote approval or disapproval of the product by Argonne National Laboratory or the U. S. Energy Research and Development Administration.

DEFECT PRODUCTION BY ENERGETIC PARTICLE BOMBARDMENT*

K. L. Merkle
Materials Science Division
Argonne National Laboratory
Argonne, Illinois 60439 USA

RECEIVED
MAY 1978

Energetic-particle irradiation of metals in most cases results in a rather complex mixture of defect structures. This variety of the microscopic arrangement of the displaced atoms and the respective vacant lattice sites is obtained generally even at low dose and in the absence of long-range migration of defects.

The present paper is a review of selected aspects of low dose, low-temperature irradiation experiments, and elevated-temperature experiments that do not involve the interaction of defects through long-range migration. In other words, we are concerned here only with the primary damage state, i.e., the situation that exists after the energy of the primary knock-on has been shared with the lattice to the extent that no excess kinetic energy is retained in the region where displacements have taken place. Since the dynamical development of the cascade takes place in times considerably shorter ($\sim 10^{-12}$ s) (1) than the times required for a defect measurement (> 1 s), the observed damage state includes effects that result from the collapse of unstable defect configurations. In elevated-temperature irradiations some short-term annealing also takes place before the observations are made.

For discussion in the present paper, we have selected such experiments that seem to be most useful in providing a basis for a quantitative description of the amount and type of damage which is obtained under a variety of irradiation conditions. Therefore, we strongly focus on experiments relating to the energy dependence of defect production. Ideally, one would like to be able to predict from experimental data the defect production that is expected for any given irradiation condition. At present, such predictions rely heavily on

*Work supported by the U. S. Energy Research and Development Administration.

theoretical models, as discussed by Robinson (2). Experimentally, considerable progress has been made in the observation of cascade defect structures by field-ion microscopy (FIM), as discussed by Seidman (3), and by transmission electron microscopy (TEM) as presented in the present paper. However, few of the comparisons of measured defect production with theory are sufficiently quantitative. As we shall discuss, significant progress has been made recently in quantifying low-energy damage production, as well as in understanding cascade effects, and quantitatively relating cascade production during ion bombardment to neutron damage results.

The present review consists of four sections. In the first, experimental methods for determining the displacement threshold are reviewed. In the second section, multiple displacements and damage rates observed by residual resistivity measurements are examined. The third section is a discussion of ion-damage studies of energetic displacement cascades by means of TEM. Finally, we discuss and compare results from TEM studies of ion and neutron damage.

PARTICLE IRRADIATION EXPERIMENTS

A solid may be affected in two ways by energetic-particle bombardment.

1. Lattice atoms are removed from their regular lattice sites; displacement damage is produced.

2. The irradiating particle can cause changes in chemical composition of the target via ion implantation or transmutations.

In the present paper we shall only be concerned with displacement production. The displacement production is best viewed as a two-step process. In the first instance, the irradiating particle (e^- , p , n , d , He^+ , etc.) interacts with the nucleus of a lattice atom. This collision process takes place within a short time (generally $\sim 10^{-17}$ s). At the end of this period, the struck lattice atom [primary atom or primary knock-on atom (PKA)] has received a certain amount of kinetic energy, but the atom has not left its normal position. In the second part of the defect production process, the primary atom leaves its lattice site and is slowed down by a series of collisions. If the energy is sufficiently high, a displacement cascade is initiated by the primary atom. In this manner a great number of secondary displacements can be generated within a local region (typically ~ 1000 Å) in the lattice. As mentioned above, the resultant defect structure is observed only after some time has passed and the defects generated in such an event have had a chance to interact with each other.

Basically, as pointed out by Robinson in the first chapter of this volume, the PKA production is rather well known for a wide range of irradiation conditions. Experimentally, the recoil-energy distribution can be obtained from measurements of the differential scattering cross section of the scattered particle, in the case of elastic collisions, via the well-known relation $E_R = E_{\max} \sin^2 \theta / 2$. Here E_R is the recoil energy, $E_{\max} = E M_1 M_2 / (M_1 + M_2)$ is the maximum energy transfer between a particle of mass M_1 and energy E and a lattice atom of mass M_2 , and θ is the scattering angle in the center-of-mass system. For a discussion of nonelastic collisions, the reader should refer to Ref. 2. In this manner, we can obtain the differential recoil cross section

$$d\sigma(E_R)/dE_R = K(E, E_R) \quad (1)$$

$K(E, E_R)$ gives the probability that a particle of laboratory energy E produces a recoil with energy between E_R and $E_R + dE_R$.

Given the number of PKA's per incident particle and the PKA energy distribution, the next step is to find the damage structure that is produced at a given PKA energy. In radiation-damage experiments, one is interested in the range of recoil energy from a few electron volts to 10^4 eV. The lowest PKA energies are not sufficient to have an atom permanently displaced from its site, but a closely spaced interstitial and a vacancy (Frenkel pair) may be recombined by such a subthreshold collision. As the energy increases, single displacements become possible above the threshold energy E_d , and, at still higher energies, first multiple displacements will be produced, then displacement cascades with a depleted zone structure, and finally splitting into sub-cascades is observed.

The description of the damage produced by a given PKA involves the total number of defects produced by this recoil as well as various other parameters that may be necessary for a complete description of the damage produced. Let us assume that the recoil energy E_R causes, on the average, a certain number of defects of a given type. This depends on the recoil energy and may be described by a damage-parameter function $g(E_R)$. The most obvious parameter of interest is the average number of Frenkel pairs $\bar{n}(E_R)$ that are produced by a recoil of energy E_R . Other parameters of interest are, for example, the number of depleted zone clusters or the number of free interstitials and vacancies that are produced in a cascade. This type of approach has been used by Beeler (4) and Parkin and Goland (5) in theoretical damage calculations. As long as a specific measurement exists for the

defect parameter in question, this same approach can be applied to the defect-production experiment.

Given the damage parameter $g(E_R)$ as a function of recoil energy, we can now determine a damage-parameter cross section for irradiation with a particle of energy E

$$\sigma_g(E) = \int_{E_R} g(E_R) K(E, E_R) dE_R. \quad (2)$$

If, as for example in a reactor, a spectrum of particles $\phi(E)$ is present we must integrate also over all incident particle energies, and we have

$$\sigma_g = \int_E \int_{E_R} \phi(E) g(E_R) K(E, E_R) dE_R dE. \quad (3)$$

This gives the effective damage-parameter cross section for the particle spectrum $\phi(E)$.

It is obvious from Eqs. (2) and (3) that the central problem in damage production is the determination of $g(E_R)$, in other words, the determination of the number of defects and defect structure as a function of PKA energy. If $g(E_R)$ is known, one can universally predict the defect-production cross sections for any irradiation for which the incident particle spectrum $\phi(E)$ and the differential recoil cross section $K(E, E_R)$ are known.

How is one to extract $g(E_R)$ from defect-production experiments? One approach is obvious from Eq. (2); a set of measurements of $\sigma_g(E)$ as a function of energy can yield $g(E_R)$ by unfolding Eq. (2). This approach is rather limited; it only works well if $g(E_R)$ shows a threshold-type behavior, i.e., if g changes from 0 to 1 in a limited energy range. Examples of this will be given during the discussions of the threshold displacement experiments and the threshold for observable depleted zone clusters. The basic difficulty lies in the fact that energy-dependence measurements using monoenergetic particles can only be done realistically with charged particles. In this case because of the Coulomb-type interaction [$K(E, E_R) \sim 1/E_R^2$], low-energy recoil events dominate and, therefore, details of the damage at higher recoil energies are extremely difficult to extract from the experimental data.

A different way of obtaining recoil-energy-dependent information is through self-ion irradiation. Figure 1 shows a comparison between recoil damage and self-ion damage. In light particle irradiations, a mixture of recoil energies ranging from E_d up to E_{max} is always obtained, but in self-ion bombardment monoenergetic cascades are produced.

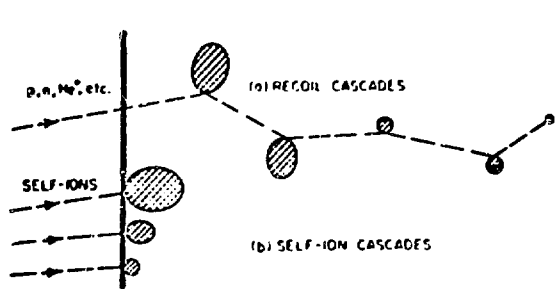


Fig. 1. Schematic View of Damage Regions Produced by Recoil Atoms and Self-Ions at Various Energies.

to the surface, some caution is advisable, especially at low energies where surface effects might strongly perturb the observations. Another difference between self-ion and recoil damage is given by the fact that self-ions do not start from a lattice position. Therefore, lattice steering effects (channeling and quasi-channeling) may be more pronounced in self-ion irradiations and such effects will be a strong function of the incident direction. The close proximity of the damage to a surface has limited experimental observations of self-ion damage to FIM and TEM studies (3,6-8). However, recently electrical resistivity measurements on self-ion cascades have also become possible (9,10).

Therefore, damage parameters are directly obtained as a function of primary energy. In Eq. (2) $E = E_R$ and $\sigma_g(E) = g(E)$. Recently, this approach has proved to be useful in studies of displacement cascades. Since the damage is introduced quite close

DETERMINATION OF THE ATOMIC DISPLACEMENT THRESHOLD

The atomic displacement threshold is the primary quantity for defect-production experiments. It is used in calculating damage rates (dpa/s), and, in the theory of atomic displacement processes, it has in the past served as a guide in the selection of the proper interatomic potential for damage calculations (1).

In the present section, we shall only be able to touch briefly on some of the more important aspects of displacement threshold determinations. For more detailed discussions of displacement-threshold-energy determinations, the reader should consult the more comprehensive reviews that have been published in recent years (11-15).

The atomic displacement threshold is defined as the minimum PKA energy necessary to produce a stable Frenkel pair. Since the separation of vacancies and interstitials proceeds via atomic replacement chains (1-3) considerably less energy is required near close-packed rows to generate an interstitial sufficiently far from its vacancy to prevent spontaneous recombination. This dependence of the threshold energy on

crystal direction, as predicted earlier by computer calculations (1,16), has in the past few years found detailed experimental attention (17-22). The minimum threshold energy E_d^{min} has also been found to follow an inverse relationship with the interatomic distance for elements within the same period of the periodic table (14), as is expected for a replacement collision mechanism (23).

Threshold-energy determinations are obtained by monitoring the changes in residual electrical resistivity per unit of dose as a function of electron energy. Threshold experiments for most materials have been performed on polycrystalline specimens. Single-crystal measurements have been made on a few metals, including Cu, Pt, Mo, Ta, Fe, Co, Zn, and Cd (17-22). The maximum transferred energy E_{max} to a nucleus of mass M_2 increases with electron energy E according to $E_{\text{max}} = 2E(E + 2mc^2)/M_2c^2$, where c is the velocity of light, and m is the electron rest mass. As E_{max} increases, a finite damage rate is observed above a certain minimum value. Displacement threshold energies are often derived from the damage rate versus PKA energy data by extrapolation to zero damage.

Although in some metals, as for example platinum (14), a reasonably sharp onset of damage is observed, others do not show such a simple behavior. Bauer and Sosin (24), for example, find in Cu and Au a long tail of "subthreshold damage" extending to rather low displacement energies. This "subthreshold damage" was shown to be strongly influenced by impurities and cold work (24). As a result of their smaller mass, light impurity atoms can receive considerably higher recoil energies than the host metal and therefore, cause lattice damage at energies substantially below threshold. Such an interpretation is supported by the observation of a saturable component in the damage rate at low energies (25,26). Nevertheless, very low minimum thresholds, within extremely small solid angles around particular directions may exist in such systems.

Rather than using a simple extrapolation to zero damage, the approach outlined in the previous section of deriving the damage-parameter function from energy-dependence measurements has been used in many instances. Here the damage parameter is the probability for displacement $P(E_R)$, and Eq. (2) becomes

$$\sigma(E) = \int_{E_R} P(E_R) K(E, E_R) dE_R. \quad (4)$$

The cross section for displacement $\sigma(E)$ is given by the change in Frenkel-pair concentration C_F per unit dose ϕ . When measured by the residual resistivity change Δ , we have $\sigma(E) = dC_F/d\phi = d\Delta/d\phi \cdot 1/\rho_F$ where ρ_F is the Frenkel-pair resistivity, therefore,

$$\frac{d\Delta\rho(E)}{d\phi} = \nu_F \int_{E_R} P(E_R) K(E, E_R) dE_R \quad (5)$$

It should be noted that Eq. (5) holds for all energies E that involve only single displacements. Therefore, once $P(E_R)$ is determined, the damage-rate data also give a value for the Frenkel-pair resistivity ρ_F . The usual procedure is to assume a certain shape of the threshold function and then attempt to fit to the experimental data by varying the threshold parameters. Figure 2 gives a few examples of such threshold

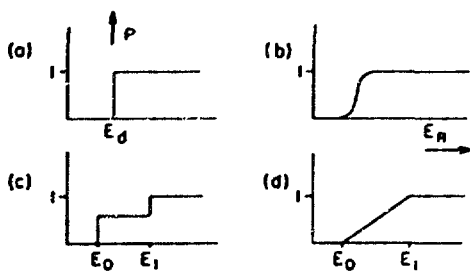


Fig. 2. Threshold functions

functions. The most simple type of function is a sharp step at E_d . As mentioned previously, a sharp threshold is not a realistic assumption. Even if the step is confined to a particular recoil direction, one expects a small but finite width to the threshold, as shown in Fig. 2b. A staircase function, as

introduced by Lucasson and Walker (27), or a linearly increasing function may be used to roughly account for the effects of the threshold anisotropy. The following observations can be made in connection with threshold determination from polycrystalline data. First, when a step function or similarly sharp rising threshold function is used, Eq. (5) generally implies unreasonably low values for ρ_F . Secondly, it is found that widely different shapes of threshold functions can give a reasonable fit to the experimental data, when ρ_F is treated as an adjustable parameter. This means that Eq. (5) cannot be used to derive $P(E_R)$ from polycrystalline data. However, if ρ_F were known accurately, the data could still give the minimum as well as an effective threshold energy. As it is, polycrystalline data give reasonably good values for the minimum threshold energy E_d^{min} , and $P(E_R)$ must be derived from single-crystal measurements. In this event, Eq. (5) is also dependent on the incident direction relative to the crystal axes. The unfolding procedure becomes quite complicated, nevertheless, Jung and co-workers (18,19) have been able to produce threshold maps that give the orientation dependence of the threshold energy in considerable detail for Ta (18) and Cu and Pt (19). Lomer and Pepper (17) have done single-crystal work on Fe, and Lucasson and co-workers (20-22) have attained data on Mo, Co, Zn, and Cd. The main problem in determining the threshold anisotropy is that damage

is always possible within a cone around the irradiation direction. Therefore, even when single crystals are used, the onset of damage is essentially determined by the displacement in the easy directions. This is particularly valid in Cu in which the minimum threshold regions are always within 20 to 25° from any crystal direction. Jung et al. (19) estimate that the observable effective threshold for any lattice direction should be lower than 23 eV in Cu, which can be compared with $E_d^{\text{min}} = 19$ eV.

For irradiations in which all directions are equally probable and cascade damage calculations, the relevant quantity is the average threshold over all crystallographic directions. It turns out that the average threshold E_d^{avg} lies about a factor of 1.5 and 2.2 above the minimum threshold, according to the Brookhaven computer model for Cu and Fe, respectively (1,16). This is in reasonable agreement with the observed ratios: 1.4 for fcc Cu and 2.2 for bcc Ta. Lucasson (15) has recently made a survey of threshold data and adopted the ratio of $E_d^{\text{avg}}/E_d^{\text{min}} = 1.4$ and 2.2, respectively, for the fcc and bcc system. Table 1 lists some values for the minimum and average threshold energies. The latter values are recommended for use in dpa calculations (2).

It should be mentioned that high-voltage electron microscopy (HVEM) has been used recently for threshold determinations. The high angular resolution and the capability to work at elevated temperature provide some interesting possibilities; however, at present, the HVEM technique requires additional development before it can yield similar or better threshold maps than are obtained in the low-temperature resistivity work. For an assessment of the present state of the art, we refer to a recent review by Urban (28).

Table 1. Atomic Displacement Threshold Energies (in eV)

	Metals							
	Al	Ni	Cu	Ag	Au	Nb	Mo	Ta
E_d^{min}	16	23	19	25	35	36	33	34
E_d^{avg}	27	33	29	39	43	78	70	90

MULTIPLE DISPLACEMENTS

If the primary atom has sufficiently high energy, it can, in turn, displace other atoms. With the exception of the region close to threshold, simple theories of multiple displacement production indicate that the number of defects $v(E_p)$ is proportional to the energy E_p available for making nuclear displacements (29,30). The most commonly used theory for

calculating the number of Frenkel pairs is the modified Kinchin and Pease model (2)

$$\nu(E_R) = \frac{0.8 E_D}{2E_d^{avg}} \quad (6)$$

Here the electronic losses Q_{e1} are subtracted from the primary energy to obtain the damage energy $E_D = E_R - Q_{e1}$. The factor of 0.8 reflects the deviations from billiard-ball scattering and is found in analytical treatments (31) as well as in computer model calculations (32).

When experimental and theoretical damage rates are compared, it is useful to introduce an efficiency factor ξ that gives the ratio of experimental-to-theoretical number of defects

$$N_F^{exp} = \xi \nu(E_R) \quad (7)$$

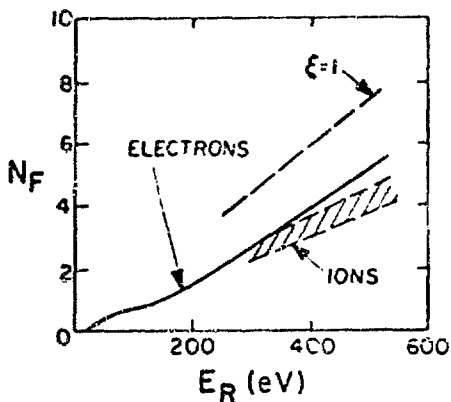


Fig. 3. Number of Frenkel Pairs N_F /PKA Produced in Electron (13) and Ion (33) Irradiation of Al.

$3.9 \times 10^{-4} \Omega\text{-cm}$, which has been derived independently from diffuse x-ray scattering experiments, (34). In general, absolute damage rates derived from electrical-resistivity measurements are not well defined because of the uncertainties in the absolute value of the Frenkel-pair resistivity in most metals. This must be kept in mind when such comparisons are made, especially since electron irradiations, with the exception of aluminum, have not been carried to high enough energies for multiple displacements to contribute significantly. As we see in the case of Al in Fig. 3, the efficiencies for both multiple displacements by electrons and charged particles fall quite close to each other (see Ref. 35) but are significantly below $\xi = 1$.

Figure 3 shows the number of Frenkel pairs in aluminum as a function of recoil energy (1) according to Eq. (6) ($\xi = 1$), (2) as derived by Wollenberger and co-workers (13) from electron-irradiation results (solid curve), and (3) the range of ξ values observed in various light-ion irradiations ($\xi = 0.52-0.66$) (33). In the latter case, the average PKA energy lies between 200 and 400 eV. These efficiency values and Fig. 3 are based on a Frenkel-pair resistivity of $\rho_F =$

The exact cause for this smaller damage rate is not known at present. It appears that more energy than indicated by Eq. (6) is required to displace the second or third atom. This seems plausible if we remember that most of the energy used to make a stable Frenkel pair goes into subthreshold events in the process of separating the interstitial far enough from its vacancy to create a stable defect. When one PKA produces two or three Frenkel pairs, they will be close to each other and therefore the chance for recombination will increase. On the average, the separations will have to be larger to create stable defects in this type of situation compared with the single displacement process. Therefore, more energy is required in the production process. The effects of such spatial correlations are not included in the simple displacement models. What fraction of the reduced efficiencies is due to this type of effect is difficult to say. E_d^{avg} may also be larger than indicated in Table 1. In this connection, it should be noted that if the threshold data were analyzed by using the same ρ_F values as in evaluating charged-particle data, one would in general obtain efficiency values that are closer to unity than the data shown in Table 2. Here the average efficiencies in p, d and He⁺ irradiations (33) ranging from 2 to 20 MeV as well as the corresponding ρ_F values are listed. Since the Coulomb interaction favors low energy transfers, the average PKA energies in these bombardments lie not far above threshold, although the maximum energy transfers can produce very energetic cascades. The efficiencies are found to be near 0.6 for the metals investigated and have little dependence on energy. The fluctuations seen in Table 1 are mainly due to experimental errors rather than some intrinsic differences.

Table 2. Damage Efficiencies

Metal	ξ		ρ_F (10^{-4} Ω -cm)
	Light-ion	Self-ion	
Al	0.52-0.66		3.9
Cu	0.58	0.42	2.0
Ag	0.62	0.45	2.1
Pt	0.57-0.66		10.0
Au	0.54-0.63	0.41	2.2

Schiøtt and Thomsen (33) have recently discussed various light-ion damage-rate measurements, using the Lindhard theory to take into account screening effects and electronic losses. Andersen and Sørensen (36) have made careful charged-particle damage-rate measurements when irradiating Au, Ag and Pt with p, d and He⁺ in the MeV region. In principle, these experiments should have yielded some information on the variation

of ξ with energy; however, no definitive conclusions could be drawn because of some uncertainties in the recoil cross sections caused by nuclear interactions and screening effects. Information on the number of defects produced in very energetic cascades is more directly obtained by self-ion bombardment. Residual resistivity measurements on self-ion cascades have recently become possible by using thin-film methods (9,10). The resultant efficiencies for self-ion cascades near 500 keV in Cu, Ag and Au are indicated in Table 2. The slightly reduced efficiency values, compared with low energy PKA's are similar in magnitude to those found in neutron irradiations (2). The smaller efficiencies may, in part, be explained by cascade effects (2,32) and, especially in the case of Au and Ag, may, in part, only be apparent as a result of the reduced resistivity contribution from clusters that are formed within a cascade (37). It should be noted that the significant electronic losses Q_{el} still introduce considerable uncertainty into the damage calculations for such energetic cascades.

In summary, we can remark that multiple displacement production within a few E_d above threshold is a largely unexplored area, and some theoretical as well as experimental work in this area is clearly needed, which would hopefully give us a firmer basis for understanding the multiple displacement processes in energetic cascades. Regarding the values of ξ , it can be said that the gap between the experiment and the simple multiple displacement theory has become more narrow in recent years. This has come about through a better understanding of the effect of realistic scattering potentials (2,31,32), the role of electronic losses (29,30), and last but not least better values for the effective threshold energy as obtained from studies of the threshold anisotropy (14,15).

TEM OF DISPLACEMENT CASCADES

In the past ten years TEM has had considerable impact on the study of radiation damage in metals. For details of the applicable methods and more general surveys, the reader is referred to the recent reviews by Wilkens (8,38), Rühle (39, 40), and Eyre (7).

TEM of Depleted Zones

We shall now be concerned with recoils that are sufficiently energetic to produce a vacancy-rich region in the center of a cascade, a so-called depleted zone (41). Such depleted zones can have rather high concentrations of vacancies, on the order of several percent (2,3). This configuration may not be stable and may collapse to a more or less planar defect cluster. Rearrangement of vacancies that result in cluster formation within the depleted zones can also

take place through thermally activated migration at finite temperatures. Most of the TEM work on cascades has been done near 300 K. The work reviewed in the following, therefore, refers to room-temperature irradiations, unless otherwise specified. Uncollapsed depleted zones usually do not have a large enough strain field to produce a visible TEM contrast. On the other hand, FIM studies (3,6) can reveal uncollapsed cascade structures with atomic resolution. Also, TEM studies are complementary to the FIM work because TEM can be used conveniently to look at more energetic and a greater number of cascades. This is of importance in view of the statistical nature of a cascade. Naturally, because of the limited resolution of TEM, cascades are seen on a relatively coarse scale: Figure 4 shows an Ag foil bombarded with 10-keV Ag^+ self-ions.

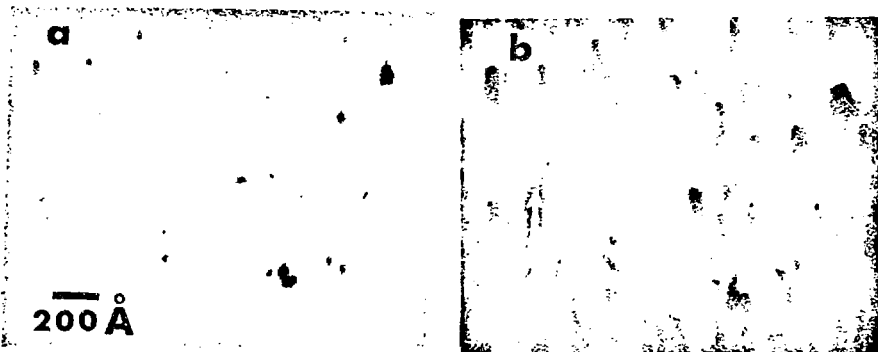


Fig. 4. Depleted-Zone Clusters in Ag, Produced by 10-keV Ag^+ Ion Bombardment. (a) Bright field, kinematical and (b) dark field, (220), dynamical.

The black-spot and black-white contrasts represent collapsed depleted zones. In this instance, not every incident ion has produced a visible cascade. Obviously one does not know a priori that these clusters are directly produced at depleted zones. Therefore, we shall, in the following, examine the conditions for the observation of such cascade structures.

1. As mentioned, the cascade must be in a collapsed state to give sufficient diffraction contrast. The collapse depends on the displacement density within the depleted zone. If this density is low enough, collapse may not take place or it might only take place with the aid of some thermal activation. For very high cascade densities, the cascade may collapse even at temperatures near 0 K. Some evidence for this is indicated through the work of Howe et al. (42). The random cascade theory (43,44) can be taken as a guide for estimating the displacement density in depleted zones and its variation with energy and mass.

2. The resultant defect must be stable. If defects are formed very close to a surface they can be unstable. In particular, glissile dislocation loops can, through image force interaction, glide through a specimen surface, and therefore a large fraction of the initially formed loops may not be observed.

3. A low dose must be used to prevent mobile defects from interacting with cascades different from the one in which they were generated. In self-ion bombardments, this condition is usually fulfilled in the dose range between 10^3 and 10^{11} ions/cm². In recoil damage situations, especially when bulk samples are irradiated, a mix of depleted zone clusters and interstitial clusters are sometimes observed even at relatively low doses. A good indication of the presence of cascade clusters is given when their numbers are proportional to the dose. Although this is a necessary criterion it is not a sufficient condition for observing isolated cascades, and care must be taken when evaluating data from high dose irradiations.

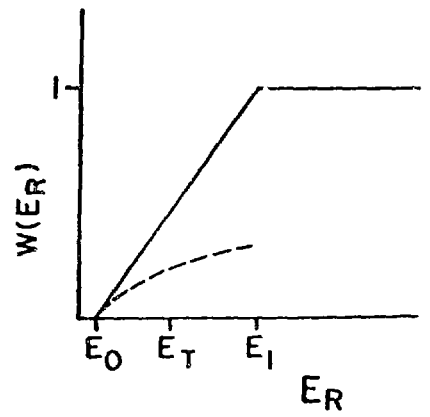
4. A minimum of 20 to 30 vacancies must be present to produce a cluster observable by TEM.

Energy Dependence

The Threshold Function (Yield Factor). Since a few tens of point defects are necessary for the formation of a visible cascade, the minimum cascade energy E_0 for which visible clusters can be expected must lie significantly above the threshold energy for atomic displacements. A lower bound for E_0 may be given by the critical defect number given in item 4. If this is used together with the modified Kinchin and Pease expression (Eq. 6), minimum energies on the order of 2 to 3 keV are obtained. Indeed, the lowest energies at which cascade clusters have been observed lie near this value. For example, Thomas et al. (45) find $E_0 = 3$ keV for self-ion bombardment of Au, Schober (46) finds cascade clusters in Ag at 5 keV and above, whereas Häussermann (47) observed Cu cascade clusters down to 6 keV.

The energy dependence of the probability for the formation of visible cascades $W(E_R)$ is schematically illustrated in Fig. 5. The cascade energy $E_C = E_R$ may either be supplied by a self-ion or a recoil atom. In some metals, each cascade is visible above a certain energy E_1 , i.e., $W(E_R) = 1$ for $E_R \geq E_1$ (solid line). In many cases, however, the probability to form a visible cluster per cascade stays well below unity up to rather high energies [dashed line in Fig. 5, which shows the case of Cu self-ion cascades (47)]. Such threshold functions are most easily determined by self-ion bombardment.

The probability for the formation of a cascade as a function of cascade energy is then simply given by the yield factor, i.e., the ratio of the number of observable cascades n_c to the number of incident ions $W(E_R) = n_c/\phi$.



However, the first derivation of such a cascade threshold function was done by Merkle (48, 49) from a study of the energy dependence of cascade cluster formation under light-ion bombardment. In this work, gold films were irradiated with protons, deuterons, He⁺ and fission fragments in the 1- to 100-MeV range. Recoil cascades were produced in this manner so that the maximum transferred energy

E_{max} varied from 10 keV to 40 MeV. A cascade cross section could be measured from the number density N_c of cascades at each energy $\sigma_c(E) = N_c/N$, where N is the atomic density. Replacing $g(E_R)$ with $W(E_R)$ in Eq. (2) and inserting the Rutherford cross section $K(E, E_R) = C_i/(E_{max}E_R^2)$, then gives

$$\sigma_s(E) = \frac{C_i}{E_{max}} \int_0^{E_{max}} W(E_R) \frac{1}{E_R^2} dE_R, \quad (8)$$

where $C_i = 4\pi e^4 Z_1^2 Z_2^2 M_1^2 / (M_1 + M_2)^2$, e is the electronic charge, and Z_1, Z_2 are atomic numbers of particle and target atoms. At energies with $E_{max} > E_1$, the details of the threshold function are of no consequence for the value of the integral in Eq. (8). Therefore, one can use an effective threshold energy E_T when working with Rutherford-type recoil spectra, and the integration of Eq. (8) gives for $E_{max} > E_1$ the simple expression

$$\sigma_s(E) = \frac{C_i}{E_{max}} (1/E_T - 1/E_{max}). \quad (9)$$

From this equation, the effective threshold energy for Au cascades was first derived from fission-fragment irradiations of Au, and a value of E_T 25 to 30 keV was obtained (50, 51). This value was later confirmed by Noggle and Den (52) in Iodine irradiations of Au. In Ref. 53 a slightly higher value

was found. As seen in Eq. (9), apart from the constant C_1 , the cascade cross section at high energies depends only on E_T and E_{max} . This is analogous to the atomic displacement threshold, where at high E_{max} the multiple displacement production is dependent on E_d^{avg} or, more accurately, on an appropriate effective displacement energy and not on E_d^{min} . It should be mentioned that the differences between E_0 and E_T have, at times, not been fully appreciated in the literature (7,45,54). In addition to this, some caution is necessary when using low keV heavy-ion experiments for measurements of the cascade threshold function. The following effects have been found by Merkle et al. (55) to influence the yield factor n_c/ϕ .

1. Since the primary atoms in self-ion bombardments are usually produced as positive ions, it has been most convenient to determine the ion dose by measuring the accumulated electric charge at the target. This method gives an apparently higher amount of damage per incident ion if a fraction of the beam becomes neutralized in charge exchange collisions with the residual gas in the beam line. Since charge exchange cross sections can be as large as 10^{-15} cm², the pressure in a typical beam line should be in the 10^{-7} Torr range if the neutral fraction is to be kept below 1%. Deflection of the ion beam just in front of the target can be used to measure the neutral component (47,55).

2. Several yield determinations have been performed with the beam incident in a channeling direction. Investigations on Au have been performed by Thomas et al. (45) Au⁺ ions in [001] direction), Högberg and Nordén (54) (Ar, Kr, Xe ions in [111]), and Merkle et al. (55) (Xe ions incident in [001], [111] and in a "random" direction). In Ref. 55 it was found that channeling influences the yield function primarily in two ways (see Fig. 6): First, at low energies (~20 keV), the yield is significantly increased when irradiating in a channeling direction. This can be explained as follows: under random incidence, low-energy cascades are centered very close to the surface. (For example, a 10-keV cascade in Au is positioned at ~20 Å from the surface according to the random cascade theory.) Therefore, the cascade may significantly intersect the surface, and the collapse of the depleted zone will be influenced by surface interactions. It is thought that at these low energies a small crater, rather than a stable cluster, is formed under random incidence (55). When irradiating in a channeling direction, the depleted zone is formed, upon dechanneling, at somewhat larger depths and the depleted zone can collapse into a stable cluster. Also, interstitials that are shot out of a cascade and deposited at or close to the surface will have a reduced chance for recombination with the depleted zone. Therefore, a region of

instability will be followed by a region in which the yield is higher than in the bulk. The latter region extends up to depths that are comparable to the range of replacement collision sequences.

The second effect of channeling on the yield is that the latter increases less rapidly with energy at high energy (see Fig. 6). This may be understood in part by energy losses while the ion travels along a channel, thus producing a less energetic cascade upon dechanneling, and by the possibility of transmission through the foil without dechanneling. Similar behavior is found in self-ion bombardment of silver. Recent threshold function determinations by Merkle and Lyles (55) have indicated that $W(E_R) = 1$ is reached in Ag under random incidence at $E_R \sim 35$ keV. This can be compared with the value of $E_1 > 50$ keV found by Schober (46) in bombardments along [001].

For a comparison of self-ion results with the average recoil cascade, the yield curve produced for random incidence should be used, except perhaps at very low cascade energies at which surface effects play a role and the true yield is expected to be between the random and channeled yield curves. In any case (Fig. 6) the Au self-ion results are in reasonably good agreement with the indirectly derived threshold function.

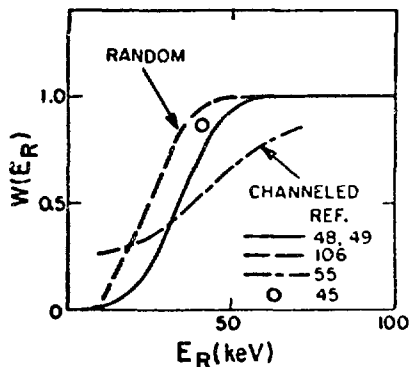


Fig. 6. Probability for Producing Visible Cascades in Au as a Function of Cascade Energy.

measurements indicated (49) that the probability P for forming a visible cascade stayed much below unity up to rather high cascade energies, with $p \sim E_T/100$ keV. This was explained by a rather strong splitting into subcascades in the case of Cu. The individual subcascades would then, in general, not contain sufficient defects to produce a collapsed depleted zone.

The latter is based on a two-parameter fit to the experimental data; therefore the recent self-ion data are expected to give a more accurate representation of the yield function. Figure 6 contains only one point of the self-ion yield data of Ref. 45, because, as the authors indicate, the other points contained errors in dose measurement, probably of the type discussed in item 1 above.

In copper, it was not possible to derive a threshold function from the light-ion data; however, the cross-section

An alternate explanation would be that the vacancy density in the depleted zones is not sufficiently high to lead to spontaneous collapse into a visible dislocation loop. Random aggregation of vacancies by thermally activated motion is likely to result in a rather disperse distribution of smaller clusters, as exemplified by computer annealing experiments (57). Self-ion bombardments by Häussermann (47) have confirmed the low yields in Cu. The same author has irradiated Cu with Au ions. In this instance, the yields are considerably higher and reach a value close to unity near 70 keV. This behavior follows from considerations of the displacement density in a cascade. Based on the random cascade theory (43,44) one would expect a cascade radius that is smaller by a factor of 2.8 for a Au cascade compared with a self-ion cascade in copper. This will considerably influence the average vacancy density as well as the possible subcascade formation. Some authors [(58) (Cu ions) and (59) (Zn ions)] have reported yields in Cu that are considerably higher than found by Häussermann (47). The yield data by the latter author, however, must be considered more reliable, since Häussermann performed his irradiations in a vacuum of 10^{-7} Torr and found that the neutral beam component was <1% of the total beam.

In Al no evidence for collapsed depleted zones has been found when irradiating with self-ions [Ruault et al. (60) and Johnson and Ytterhus (61)]; however, when irradiating with Hg [Norris (62)] or Au [Gomez-Giraldez et al. (63)], small Frank loops are observed.

In body-centered-cubic (bcc) metals cascade cluster yields are generally rather low (62-68). In Fe no vacancy clusters have been found after self-ion bombardment (65). Buswell (66) observed Hg, W, and Zn ion damage in tungsten by TEM and FIM and found that only a small fraction of the vacancy clusters collapsed to dislocation loops. This is consistent with Häussermann's (64) observations of yields on the order of 2×10^{-2} in Au ion-bombarded W. An additional complication in bcc metals is the loss of glissile vacancy loops to the surface. This effect makes the yield dependent on the surface orientation (64). Self-ion bombardments of Mo indicate a strong influence of interstitial impurities on cascade yield and cluster size (64,68). English et al. (68) found that the yield drops from 1 to 0.2 in 60-keV Mo^+ irradiation of Mo when going from high-purity material to Mo + 17 ppm nitrogen. This effect was explained on the basis of the large misfit strains associated with interstitial solutes. These strains are expected to have a significant effect on the defocussing of replacement sequences, which, in turn, reduces the separation distance between vacancies and interstitials and therefore gives rise to an increased probability of

recombination between interstitials and vacancies. The authors also remark that the impurities may influence the cascade collapse. However, in view of the small concentrations involved, this effect is not likely to control the observed behavior.

Subcascade Formation. It was first observed by Merkle et al. (50), that energetic recoil cascades in fission bombarded gold could produce several closely spaced defect clusters. This splitting into subclusters has also been observed in xenon bombarded gold (69), in Au self-ion cascades (45,70,71), in Ag self-ion cascades (56,72), and in Cu irradiated with Au ions (47).

From light-particle irradiations in which recoil cascades are produced, subcluster formation in Au was indicated at maximum PKA energies >100 keV (49). Subsequent Xe ion bombardments of Au showed the onset of subcascade formation to be between 30 and 40 keV (69). Thomas et al. (45) give 15 keV as the threshold for subcascade formation in self-ion bombardments of Au when irradiating along [001]. In contrast to this, our self-ion irradiations of Au in a random direction show the behavior indicated in Fig. 7. Here the probabilities

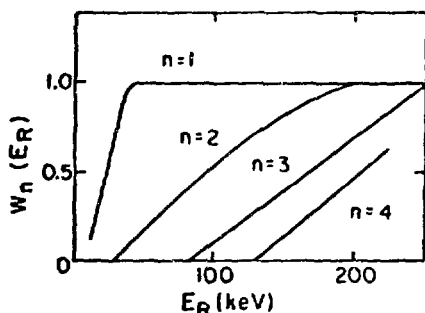



Fig. 7. The Probability for Producing n or More Visible Clusters per Au Self-Ion Cascade.

of producing at least one to three or more subclusters are plotted as a function of cascade energy. A finite probability for observation of at least two clusters exists above 30 keV, a probability of 0.5 for more than one cluster is observed at ~100 keV, and all cascades show subcluster formation above 200 keV. The information in Fig. 7 is obtained by direct examination of the images of individual isolated cascades, as seen, for example, in Fig. 8.

The average number of subclusters n increases linearly with energy in the region from 100 to 300 keV, with $n \propto E_R/70$ keV, which corresponds to $n \propto E_D/50$ keV.

A pronounced tendency for subcascade formation has been reported for Cu self-ion cascades [2.5 to 4 clusters per 150-keV Zn ion (59)]. However, those measurements were based on yield determinations only, giving much higher values than found in other investigations of Cu (47,49), and are also in contrast to the low yields found in direct observations of multiple clusters for Au on Cu (10 to 15% at 70 keV) (47).



200 Å



200 Å

Fig. 8. Subcascade Structure Observed in a 300-keV Au Self-Ion Cascade. Fig. 9. 250-keV Ag Self-Ion Cascades Produced at 523 K.

Therefore, no direct evidence exists, at present, for subcluster formation in copper, except in the dense cascades produced by Au ions. The explanation for the low yield and the absence of subcluster formation in self-ion bombarded copper must be sought in the incomplete cascade collapse and, possibly, in the presence of small subcascade regions that are too small to result in the formation of a visible cluster.

Since the concept of a subcascade is not without ambiguities, some care must be taken when relating the observed splitting into subclusters to the detailed structure of a cascade as generated. In connection with TEM observations, a subcascade may be defined as a finite more or less spherical region of substantially higher than average vacancy density within a cascade. If such a region is of sufficient size and contains a high enough density of vacancies, it meets the criterion for the spontaneous formation of a visible depleted-zone cluster. A cascade can therefore give rise to several subclusters if such a division in several depleted zones takes place. In addition to clusters, uncollapsed depleted zones may be present within a cascade.

The basic reason for the splitting into subcascades comes from the fact that the nuclear collision cross sections increase with a decrease in energy. The densest cascades are therefore always produced at low energy. Secondary recoils of keV energies usually produce damage regions that strongly overlap and therefore do not give rise to individual subcascades. But, as the cascade energy increases, the mean free path between energetic collisions also increases. This eventually leads to well-separated depleted zones. An extreme example for this is fission fragment bombardment. Since the target atom and the fission-fragment mass are of similar

magnitude, we can view a fission fragment as a primary ion that initiates a very energetic (~ 100 MeV) displacement cascade. It is well known that spatially well-separated cascades (or subcascades in the present terminology) are formed in this case (51), and the damage distribution is quite similar to the recoil case, as shown in Fig. 1a. In fact, many of these secondary recoils produced along the path of a fission fragment in Au were sufficiently energetic to provide the first experimental indication of subcascade formation (50), or sub-subcascades in the present context. This observation shows that subcascade formation is a universal feature of energetic cascades. We can also deduce from random cascade theory (44) that considerable fluctuations of defect densities exist within energetic cascades. In this theory, the energy deposition for an amorphous solid is calculated. When electronic stopping is neglected, a cascade radius proportional to $E^{2/3}$ or E for low and high cascade energies, respectively, is derived, giving a defect density proportional to E^{-1} or E^{-2} , respectively. Given an energetic cascade to say $E_c = 300$ keV, it is clear that a secondary recoil of 30 keV that takes place within this cascade will produce a local defect density that is at least a factor of ten higher than the average in this cascade. Since such secondary recoils occur with a finite probability, we see that isolated depleted zones can be formed in such energetic cascades. Distinctly separated regions of displacements have recently also been found in binary collision cascade calculations (73). The separation into subcascades is aided by channeling. Beeler (74) defines quasi-channeling as channeling over distances < 1000 Å. In such an event, the primary or an energetic secondary atom is scattered into a channel and travels a small distance in the channel. Upon dechanneling, a subcascade is formed. Attempts to correlate the spatial position of subclusters to crystallographic channeling trajectories have not been conclusive to date (45,69).

An important consequence of the subcascade formation is that interference effects are reduced in very energetic cascades. The basic subunit of the damage, the subcascade, stays the same with increasing energy. As a consequence, the separation of interstitials and vacancies takes place over the same distances. The high concentration of interstitials in between subcascades may give rise to the nucleation of stable interstitial clusters. So far none have been identified in connection with isolated energetic cascades.

Finally, it must be remembered that the TEM observations of depleted zone clusters give only a very rough and simplified view of a cascade. Since only the collapsed cores of depleted zones are visible, the separation of closely

spaced subcascades is exaggerated, and the strong irregularities on an atomic scale that are seen in machine calculations and FIM are lost. The recently developed technique of observing the disordered regions in Cu_3Au by TEM gives a more direct view of the damage volume in energetic cascades (8,75).

Defect Structure

Several TEM imaging techniques have been developed in recent years that allow the characterization of small defect clusters. For details the reader is referred to several recent reviews (7,8,38-40,76-78). Basically, the approach has been that of computer modeling of images for given defect clusters and comparing the computer images with experimental observations. In addition to this, symmetry considerations have often been used to analyze defect-cluster images.

Standard TEM imaging conditions include kinematical bright field, dynamical bright field and dark field, weak-beam dark field, and the out-of-focus technique.

Determination of Defect Type. TEM imaging techniques can be used to determine the sign of the misfit volume associated with defect clusters. The nature of large, resolvable dislocation loops can be analyzed by the "inside-outside" method (76). Cascade clusters are, however, mostly unresolved. In this case, the black-white contrast method developed by Rühle et al. (79) is applicable. Under dynamical bright or dark-field conditions, small defect clusters exhibit characteristic black-white contrasts; the direction relative to the diffraction vector depends on the sign of the misfit volume. The direction of the black-white contrast also depends in an oscillatory fashion on the distance of the cluster to the nearest surface. Therefore, in general, a mix of black-white contrast directions is observed even if only one type of defect is present, and to determine the nature of individual defects, the depth position must be known. This can be measured via the stereotechnique (39,40). Only in the case where all defects have the same sign of the misfit volume and lie close to one surface can one obtain black-white contrasts of only one sign. This is shown in Fig. 4b, where 10-keV Ag^+ cascades were produced close to the surface and practically all the black-white contrasts point in the direction consistent with the vacancy nature of the cluster. A number of black-white contrast investigations have shown that the cascade clusters in Au, Ag, Cu, Al, Mo, W, and Co are of the vacancy type (8,42,45-47,49, 62-64,80,81) when the conditions for formation of isolated cascades are met. In some cases, interstitial clusters have been identified but in these instances, doses are usually relatively high and linearity of cluster density with dose is not observed (69,61,82).

Recently, the so-called 2-1/2 D method for the determination of the nature of small dislocation loops has been introduced (83). At present, this method is still in the development stage, but it has the possibility of simplifying the character determination of small defect clusters.

Defect Morphology. TEM contrast experiments can reveal structural details of the vacancy clusters. It was found that, in fcc metals, most vacancy clusters can be identified as dislocation loops of the Frank type with a Burgers vector $b = 1/3 \langle 111 \rangle$ (7,8). In many instances, the contrast behavior shows deviations from the ideal loop contrast. Dissociated Frank loops as well as some incomplete and complete stacking-fault tetrahedra have been found in Cu, Ag, and Au (81,46). The tendency to form stacking-fault tetrahedra is enhanced at elevated temperature (37,67). On the other hand, Howe, et al. (42) have reported formation of Frank loops in Cu and Au when bombarded with 100-keV O^- ions at temperatures as low as 20 K. In self-ion bombardments at energies below 10 keV, some cascades show no preferential direction of the strain field in Au (45), Ag (46), and Cu (47).

Referring to bcc metals, it is found that perfect dislocation loops are formed in Mo and W. Most of the loops lie on (110) planes with $b = 1/2 \langle 111 \rangle$ (64,67). Such loops are glissile and can therefore be attracted to the surface by image forces. The loss of loops through the surface depends on the surface orientation. From the population of loops on differently oriented foils, Häussermann (64) concluded that the loops are formed by a two-step mechanism. Initially, the cascade collapses to a Frank loop: $b = 1/2 \langle 110 \rangle$ on (110). Then the Frank loop is converted by a shear $\pm 1/2 \langle 001 \rangle$ into a perfect loop ($b = 1/2 \langle 111 \rangle$). Which of the two possible shear components is activated depends on the position of the adjacent free surface.

Since in these systems the Burgers vector is inclined to the habit plane of the dislocation loop, the TEM contrast analysis is fairly complicated due to the multitude of possible habit planes and Burgers vectors (84). When hcp Co is bombarded with 40 to 60-keV Au ions, vacancy loops with shear components have been found, most of which could be indexed with $b = 1/3 \langle 11\bar{2}0 \rangle$ on $\{1100\}$ planes (8).

Size Distribution

Cluster size distributions have been studied in Au and Cu by Merkle (49,69), Thomas et al. (45), Pronko and Merkle (70), Häussermann (47), and Wilson (58). In Au, an increase in mean cluster size with mean cascade energy is observed (45,49,69). In self-ion irradiations of Au, the cluster size

increases relatively quickly up to ~ 50 keV. Above this energy, only a slight increase in mean cluster size with energy occurs. This is due to the splitting into subcascades, which proceeds rather linearly with damage energy. Therefore, the size of individual subcascades stays almost constant with increasing cascade energy (85).

In copper self-ion bombardments, Wilson (58) finds no significant change in the size distribution when going from 30 to 90 keV, which is in agreement with other observations (49). For Au^+ bombardment of Cu, an increase in cluster size has been found in the region up to 70 keV (47). When 70-keV Au ions are incident along a [001] channel, the observed cluster size decreases with depth below the surface.

Clustering Efficiency. Obviously the number of vacancies in a cluster can be determined from its geometry and size. Unfortunately, the geometry and size of very small black-spot defect clusters are not well defined. The measured diameter is dependent to some extent on imaging conditions (77). Usually, kinematical conditions are used for imaging (Figs. 4a, 8, and 9), and the measured diameters are reduced by a factor of 1.2 (39). The number of vacancies in visible clusters \bar{N}_V can be compared with the number of vacancies $\nu(E_R)$ predicted by a modified Kinchin and Pease model [Eq. (6)]. To this end, a cascade efficiency $\xi = \bar{N}_V/\nu(E_R)$, as in Eq. (7), is defined.

In Au, Ag, Cu and Mo, cascade efficiencies on the order of 0.5 or more are observed (69,56,47,68). In self-ion bombardments of Au, the efficiency stays rather constant in the energy range to 300 keV, except in the region below 50 keV. However, in this low-energy region, not all cascades produce a visible cluster. If the invisible cascades are also taken into account, i.e., if the average efficiency per incident ion is determined, the efficiency values are close to the values found at high energy. It should be noted that, in previous determinations of cascade efficiencies, comparisons were usually made with a simple modified Kinchin and Pease expression in which the minimum threshold energy was used and also the factor of 0.8 in Eq. (6) was neglected. To be consistent with the present definition of ξ , these earlier efficiencies should therefore be multiplied by a factor of 1.75 for fcc metals.

Recently, yields and efficiencies have also been measured on cascades produced at elevated temperatures (37,67,71). It is found that yield and efficiencies stay rather constant up to the point where cascade clusters begin to dissolve by thermal evaporation of vacancies. Figure 9 shows an example of an Ag foil irradiated with 250-keV Ag^+ ions at 523 K. Individual cascades show sub-cascade formation and relatively

well-defined, resolved dislocation loops and stacking-fault tetrahedra. This more regular appearance of the defect structure, compared with room-temperature irradiations, indicates that considerable rearrangement of defects within the depleted zones has taken place at elevated temperature. When viewing these relatively large and regular clusters, it is possible to deduce the defect content with a much greater amount of confidence than would be possible for black-spot clusters that lie just above the visibility limit. Nevertheless, the vacancy content of these high-temperature cascades is roughly the same as of the ones as found at room temperature. This gives some confidence to the vacancy values obtained from black-spot size measurements and, at the same time, shows that the mechanisms for separating vacancies and interstitials also work very effectively at temperatures where both interstitials and vacancies are highly mobile.

Apart from looking at the average cascade efficiencies, it is also possible to examine the distribution of vacancy content in individual cascades, which is shown in Fig. 10. Some of the cascades are seen to contain as many or more vacancies than expected from the modified Kinchin and Pease

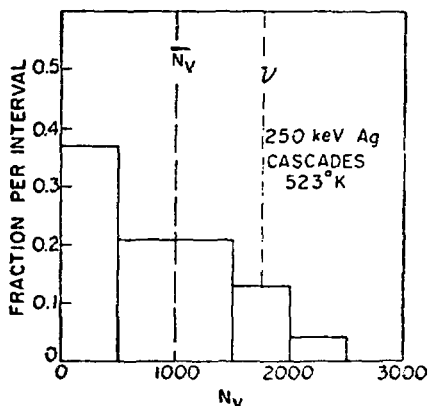


Fig 10. Distribution in the Number of Vacancies Clustered in 250-keV Ag Cascades.

theory. This is quite remarkable because it not only indicates a strong tendency to form defect clusters but, in addition, shows that almost all of the vacancies formed in some cascades can be in the form of large clusters. This also implies that no large fraction of the vacancies and interstitials recombine within the cascade. Interstitials must, therefore, be separated at generation over distances comparable to or larger than the size of a depleted zone.

It has been argued that the use of thin films for in-

vestigations of cascade damage favors the formation of vacancy clusters over interstitial clusters because interstitials can easily reach a surface either by dynamic propagation or by thermal migration. The question that arises is how many of the interstitials that end up at the surface would, if produced in the bulk, have been able to return to the depleted zone, annihilate, and thus reduce the size of the vacancy cluster. A defect at distance r from the

depleted zone of radius r_0 will return to the depleted zone with a probability of $p \sim r_0/r$, if the defect performs a three-dimensional random walk. Typical depleted-zone sizes are below 50 Å in radius, and thus, at distances >100 Å from the surface, the influence of the surface on the return probability of interstitials should be negligible. However, for one-dimensional diffusion (Crowdion migration), the return probability of interstitials is always unity in the ideal infinite lattice. In this case, the return probabilities may be strongly reduced by the introduction of a surface, especially if the initial separation of the interstitials from the depleted zone is comparable to the film thickness.

In bulk irradiations the primary damage structures can be disturbed by freely migrating interstitials that may form interstitial clusters and reduce the size of existing vacancy clusters. Quantitative comparisons between cascade-damage structures produced in the same recoil spectrum on thin film and bulk specimens have not been made to date.

Cascade Volume. As previously mentioned, the size of the small clusters bears no direct relationship to the size of a depleted zone. However, in addition to producing TEM images that are due to the strains associated with small defect clusters, Wilkens and co-workers (8,75) have recently observed the regions of disorder associated with displacement cascades in order Cu_3Au . In this work, superlattice reflections are used to image local regions of disorder associated with depleted zones. The size of these regions directly relates to the size of those regions within a cascade that contain a considerable amount of disorder. Depleted zone sizes derived in this manner seem to be in reasonable agreement with the random cascade theory (86).

The location of the depleted-zone clusters can give some indication of the transverse extension of a cascade when several subclusters are formed per cascade. This, together with the depth distribution can give the spatial extension of a cascade, although the sizes of individual clusters are only indicative of the number of vacancies in a depleted zone.

Depth Distribution

A number of investigators have used the stereomethod (40) to determine the depth distribution of the damage in self-ion bombardments or irradiations with other heavy ions. Thomas et al. (45) have irradiated Au with Au ions parallel to axial channeling directions. When bombarding parallel to (001), these authors find that the tails of the cluster depth distributions agree rather well with the range data of Whitton (87). Similarly channeled damage depth distributions were

observed in self-ion bombardment of silver (46). When the primary atom is incident along a channel, it can travel over distances much larger than the amorphous range. Also, because a strong tendency for dechanneling exists most self-ions still have a considerable amount of energy when they are dechanneled. At this point, a random cascade is produced, and, since the amorphous range is only slightly larger than the distance to the center of the depleted zone, the channeled damage distributions essentially agree with the range distribution of the channeled ions. Channeled primary atoms are almost never produced in recoil cascades because the primary atom starts at a lattice position and is ejected in a more or less random direction. Therefore, random incidence must be used when simulating recoil cascades by self-ion bombardment. Considerable difficulties are connected with choosing a truly random direction, since the critical angles for channeling can be on the order of 10° for self-ion irradiations.

Norris (88), after irradiating into unspecified random directions, concludes that his data for Au (150-keV Hg^+ and 80-keV Au^+ ions) and Cu (150-keV Cu^+ and 150-keV Au^+ ions) show good agreement with the random theory. However, the median cluster depth in Au at 150 keV that was found by Norris is significantly larger than the mean damage depth in the random model (44). The same author finds that the median cluster depth in Ni bombarded with 150-keV Hg^+ ions is a factor of two smaller than the value obtained from the random cascade theory. Since no explanation for this kind of behavior exists, verification of this result seems necessary. Merkle and co-workers (70,85) have irradiated Au with self-ions in random directions and observed that the damage distributions are centered at considerably larger depths than predicted by the random cascade theory. These measurements are supported by results from damage depth distribution measurements by means of the channeling-effect method (70), but are in contrast to TEM stereomeasurements by Ruault et al. (82) who find reasonably good agreement with the random cascade theory. The observed deviations from the random theory may be partly due to some unavoidable channeling of the incident beam; however, it is believed that channeling or quasi-channeling of energetic secondaries can also lead to an increased separation between subcascades. In Cu, depth distributions of 30-keV self-ion irradiation damage in a random direction and along the $\langle 110 \rangle$ channel qualitatively show the effect of channeling on depth distribution (58). However, the cluster-depth distribution in the random direction is peaked at a considerably smaller depth than predicted by the random theory. In self-ion irradiations of Al, no depleted-zone clusters are observed, however, depth

distributions of interstitial clusters that develop at high dose are in agreement with the random theory (60,61). In conclusion, we can say that the TEM stereo-method is a valuable tool for looking at damage depth distributions. However, to date, the experimental conditions have not been sufficiently controlled (especially the incident-beam direction) to allow definitive conclusions regarding the magnitude of the deviations in random cascade size from theory. In a few instances (Cu and Ni), cluster visibility variations with depth may distort the observed distributions.

Channeling

Channeling of the incident beam influences the damage production mainly in two ways: the damage is deposited over a greater depth, and a reduction in damage rate is observed. The former effect has been discussed in the preceding section. Regarding the reduction in damage rate, one must distinguish between cascade damage (self-ion irradiations in the 100-keV region and below) and recoil damage (light- and heavy-ion damage in the MeV range). The total number of displacements produced in a cascade is only slightly influenced by channeling, since, in general, low-energy heavy particles dechannel before losing a significant amount of energy. In addition to this, self-ions may produce displacements in the channeled condition (89,90). In contrast to this, the number of energetic recoils produced by a penetrating beam of particles can be strongly affected by channeling. Here the steering action of the atomic-row potential prevents the channeled particle from coming close to the nuclei, thus eliminating high-energy recoils. The residual damage that is observed in a perfectly aligned crystal is due to the fraction of the beam which is not channeled. The latter component is due to ions scattered by surface atoms and string atoms that are displaced from the ideal row via thermal vibrations. The influence of channeling on the production of cascade clusters in Au has been investigated by Noggle and co-workers (52,91). When Au is irradiated with 51-MeV iodine ions, a reduction in the damage rate by more than an order of magnitude was found when going through the [001] axial channel. A similar drop in damage yield has recently been found in He bombardments of Au along [001] (71,85). In the latter case, the damage is strongly enhanced near the incoming surface. This is due to recoiling surface atoms that in contrast to the atoms below the surface do not experience a reduction of close nuclear encounters.

TEM observations of cascade clusters have also been used to study the dechanneling at stacking faults and microtwins (69,71,92-94) and to study the energy loss of channeled ions (64).

COMPARISON BETWEEN CASCADE STRUCTURES OBSERVED
IN NEUTRON AND ION IRRADIATIONS

Following the first black-spot observation by Silcox and Hirsch (95) in fast-neutron-irradiated copper, a great number of TEM investigations of neutron-irradiated metals have been performed. Most irradiations have been done on bulk specimens that were thinned electrochemically after irradiation. Consequently, in addition to depleted-zone vacancy clusters, interstitial clusters are also present in most neutron-irradiated samples. In copper, the most extensively studied metal (96-100), the vacancy clusters are always found at the small end of the size spectrum, and the larger loops are invariably of the interstitial type. The ratio between the number densities of interstitial and vacancy loops differs widely among investigations. This is not too surprising since, for example, differences in impurity level, temperature, sample size play a role in the interstitial loop nucleation. A background density of small depleted-zone clusters should depend mainly on the neutron spectrum and linearly on dose. A nearly linear increase with dose is observed by Makin (96) and Rühle (97), and the observed cluster densities per incident neutron are of similar magnitude. For a quantitative comparison with self-ion results, it is necessary to have, in addition to careful neutron dosimetry, a good knowledge of the recoil spectrum. Detailed calculations of the neutron and recoil spectrum for the Cu irradiations have not been performed, therefore, relatively rough estimates only confirm the order of magnitude of agreement (97). It should be noted that the small defect clusters in Cu have not always been observed (100). Apparently in this instance, depleted-zone clusters lie below the visibility limit. This points out an inherent difficulty when using Cu as a test case, because here most depleted-zone clusters lie so close to the visibility limit that small fluctuations in the instrumental resolution or reduction of the size of existing vacancy clusters by absorption of interstitials cause a large change in the observed number density of vacancy loops.

This problem does not exist in the case of Au or Ag, where the cluster size distributions extend well above the visibility limit and every cascade above a certain energy E, produces a visible defect (49,56). Before proceeding to a discussion of the quantitative aspects of damage production in Au and Ag, we shall briefly mention some of the relevant findings after neutron irradiation in these and other metals. For more detail, the reader is referred to some recent reviews (7,38,39).

It was established in Cu, Ni, and Au that the small loops were of the vacancy type (97,101,102,62). The vacancy clusters were identified to be, for the most part, of Frank type, which is in agreement with the self-ion studies of fcc metals. In neutron-irradiated bcc metals, the situation is somewhat more complicated. The most detailed studies have been performed by Mo by Eyre (7) and co-workers. In general, more interstitial clusters are observed than vacancy clusters. The density of vacancy clusters per incident neutron is significantly below that observed in fcc metals. The observed vacancy clusters density also depends on the purity. The low yield as well as the dependence on interstitial impurities are consistent with the observations after self-ion bombardment. Nb and Mo have a similar behavior, with both vacancy and interstitial loops observed (13,103,104). Mitchell et al. (105) have investigated 14-MeV neutron damage in Nb. They conclude that 14-MeV neutrons produce a substantially higher number of defect clusters than reactor neutrons. The low yield of cascade clusters that is generally observed in bcc metals and the striking influence of interstitial impurities on cluster formation have, up to now, discouraged attempts at a detailed quantitative comparison between self-ion and neutron-induced cascade structures in these metals.

Quantitative comparisons between ion and neutron damage in Au were made in Refs. (48) and (106). In this instance, $g(E_R) = W(E_R)$ and from Eq. (3) we obtain the cross section for producing visible cascades σ_S

$$\sigma_S = \int_E \int_{E_R} \phi(E) W(E_R) K(E, E_R) dE_R dE. \quad (10)$$

The differential cross section $K(E, E_R)$ is divided into two parts, depending on the type of collision that occurs between the neutron and the nucleus

$$K(E, E_R) = K_{el}(E, E_R) + K_{nonel}(E, E_R) \quad (11)$$

In elastic scattering events, the total amount of kinetic energy is conserved, whereas, in nonelastic collisions, the neutron is initially absorbed into the nucleus followed by the emission of one or more particles. Since these recoil events are discussed by Robinson (2), it suffices to say that non-elastic collisions dominate the defect production at high neutron energies (> 10 MeV) and always result in very energetic cascades for which the average energy lies slightly above $E_{max}/4$. Figure 11 shows the neutron spectra used in Refs. (48) and (106), and Fig. 12 gives the corresponding recoil

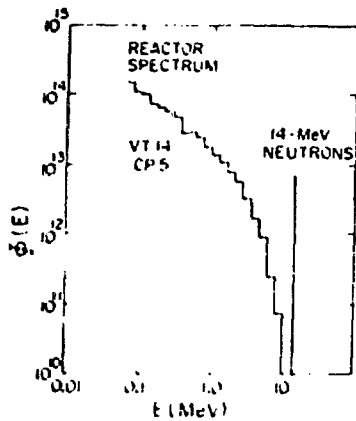


Fig. 11. Shape of Neutron Spectra Used in Irradiations of Refs. (48) and (106).

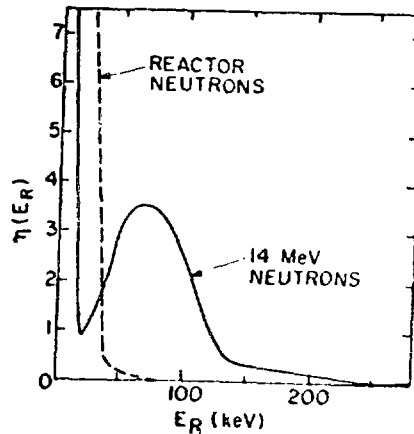


Fig. 12. Recoil Density (Arbitrary Units) for Reactor Neutron (48) and 14-MeV Neutron (107) Bombardment of Au.

spectra $\eta(E_R) = \int E K(E, E_R) \phi(E) dE$. It can be seen that the two spectra are quite different. In the 14-MeV neutron case, almost all of the damage is produced in very energetic cascades. In particular, it was found (106) that every nonelastic event produces a visible cascade. Since the recoil spectrum extends well into the region where subcascade formation has been observed in self-ion bombardment, one also expects subcascade formation under 14-MeV neutron irradiation. This is indeed observed, as can be seen in Fig. 13. In this figure, several well-separated cascades are visible, and the splitting into subcascades is quite obvious. This is in contrast to the reactor neutron case (Fig. 14) in which only a small fraction of the cascades are expected to show subcascade formation. It should be pointed out that the density of clusters in Fig. 14 is too high to allow conclusions regarding the presence or absence of subcascades. It has been suggested that, from the presence of closely spaced spots, evidence for subcascade formation is indicated in relatively high dose 14-MeV neutron irradiation of Cu and Nb (105). This conclusion is not justified, unless such observations are also made at sufficiently low doses so that individual cascades are well separated in space. At least in the case of Cu, the self-ion results have not shown any evidence of observable subcascades. Although one expects splitting into subcascades at high cascade energies, this does not necessarily mean that these subcascades are visible by TEM. Only in those cases in which the probability of forming a visible cascade cluster

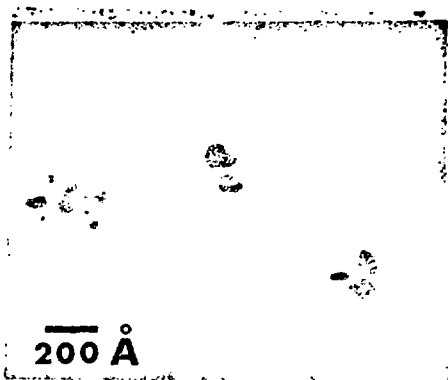


Fig. 13. 14-MeV Neutron Bom-
barded Au at 7×10^{15} n/cm².
Note subcascade formation.

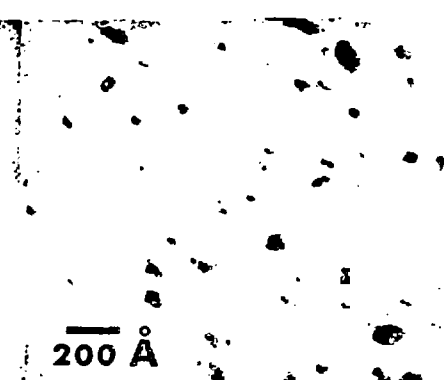


Fig. 14. Reactor Neutron Ir-
radiated Au at 6.2×10^{17} n/cm²
(>1 MeV).

reaches the value of unity at reasonably low energy (≤ 50 to 100 keV) is a readily observable subcascade structure expected. This behavior is observed in Au and Ag, and TEM evidence for subcascade formation for both metals has been found after low-dose, 14-MeV neutron bombardment (72,106).

A linear increase in cluster density with 14-MeV neutron dose has been found in Au and Ag (72,106). The corresponding cross section for the formation of visible cascades $\sigma_s = N_c/N\phi$, after reactor and 14-MeV neutron bombardment of Au, is compared in Table 3 with the theoretically predicted cross

Table 3. Cascade Damage Cross Sections, Barns (10^{-24} cm²)

Neutron Spectrum	Experimental	Theoretical			Reference
		Elastic	Nonelastic	Total	
Reactor	0.55	0.33	0.27	0.60	(48)
14-MeV	3.3	0.56	2.44	3.0	(106)

sections, based on the cascade yield function determined from ion experiments. It is seen that excellent agreement exists between the theoretical and experimental cascade production cross sections for the case of reactor neutron and 14-MeV neutron bombardments.

SUMMARY AND CONCLUSIONS

At present we have a fairly good understanding of the displacement threshold and its anisotropy. However, considerable uncertainties exist regarding the exact shape of the threshold function. Although the minimum threshold is known fairly accurately for a wide class of materials, more knowledge

concerning the effective threshold energy and the energy at which the threshold function reaches a value of unity is required. Considerable progress in this area has been made recently by studies of the threshold anisotropy.

Little is known experimentally about the multiple displacements that take place at energies not too far above threshold. It is expected that the slightly lower than predicted damage rates in ion irradiations can be understood when we have a better knowledge of the multiple displacement processes just above threshold.

TEM studies of cascade damage have yielded a rather consistent picture of the energy dependence and structure of depleted-zone clusters in a number of metals. In the heavier fcc metals, a significant fraction of the vacancies that are expected to be generated in a cascade are found to precipitate in depleted zones in the form of visible vacancy clusters, even at elevated temperature. This implies that vacancies and interstitials can be separated rather efficiently in the cascade process. At cascade energies in the 100-keV range, a strong tendency toward subcascade formation is found.

As far as the total number of defects generated is concerned, the subcascade formation can be viewed as a simplification of the cascade damage at very high cascade energies. The repetition of the basic subunit of damage and the associated reduction in cascade interference suggest that the number of defects generated should be proportional to the damage energy at very high cascade energies. This leaves the electronic losses as the major uncertainty in this range. It should be emphasized that the split cascade is structurally quite different from the single depleted-zone type found at low energy. These structural differences may be expected to influence a number of physical properties. The efficient separation of vacancies and interstitials in the pure fcc (and at least one bcc metal) metals may not take place in alloys and impure metals. This is seen very strikingly by the effects of interstitial impurities on cascade cluster yield and efficiency in Mo.

Finally one finds excellent agreement between the calculated and observed densities of cascade structures in Au for two widely different neutron spectra. This shows that accurate predictions of the primary damage can be made when the conditions for the formation of damage as a function of recoil energy are known. In this event, the threshold function for the formation of visible cascade structures was relatively well known from the results of ion bombardments. Similarly, one may expect that, when it is possible to determine the threshold function for displacement with

more precision, a closer agreement can be obtained for the predictions of the Frenkel-pair damage rates for different types of irradiations.

REFERENCES

- (1) G. B. Gibson, A. N. Goland, M. Milgram, and G. H. Vineyard, *Phys. Rev.*, Vol. 120, 1960, p. 1229.
- (2) M. T. Robinson, contribution to this volume.
- (3) D. N. Seidman, contribution to this volume.
- (4) J. R. Beeler, *J. Test. Eval.*, Vol. 3, 1975, p. 230.
- (5) D. M. Parkin and A. N. Goland, *Proceedings of International Conference on Radiation Effects and Tritium Technology for Fusion Reactors*, Gatlinburg, 1975.
- (6) D. N. Seidman, *J. Phys. F.*, Vol. 3, 1973, p. 393.
- (7) B. L. Eyre, *J. Phys. F.*, Vol. 3, 1973, p. 422.
- (8) M. Wilkens, in Applications of Ion Beams to Metals, S. T. Picraux, E. P. EerNisse, and F. L. Vook, Eds. Plenum Press, 1974, p. 441.
- (9) W. Kesternich and K. L. Merkle in Applications of Ion Beams to Metals, S. T. Picraux, E. P. EerNisse and F. L. Vook, Eds., Plenum Press, 1974, p. 495.
- (10) R. S. Averback and K. L. Merkle, *Proceedings of the International Conference on Fundamental Aspects of Radiation Damage in Metals*, Gatlinburg, 1975.
- (11) G. W. Corbett, "Electron Radiation Damage in Semiconductors and Metals," in Solid State Physics, F. Seitz and D. Turnbull, Eds., Suppl. 7, Academic Press 1966.
- (12) A. Sosin and W. Bauer, "Atomic Displacement Mechanism in Metals and Semiconductors," in Studies in Radiation Effects in Solids, G. J. Dienes, Eds., Vol. III, Gordon and Breach, 1969, p. 153.
- (13) H. G. Wollenberger, in Vacancies and Intersitials in Metals, A. Seeger, D. Schumacher, W. Schilling, and J. Diehl, Eds., North-Holland, Amsterdam, 1969, p. 215.
- (14) P. Jung, in Atomic Collisions in Solids, S. Datz, B. R. Appleton, and C. D. Moak, Eds., Vol. I, Plenum Press, 1975, p. 87.
- (15) P. Lucasson, *Proceedings of the International Conference on Fundamental Aspects of Radiation Damage in Metals*, Gatlinburg, 1975.
- (16) C. Erginsoy, G. H. Vineyard, and A. Englert, *Phys. Rev.*, Vol. 133A, 1964, p. 595.
- (17) J. N. Lomer and M. Pepper, *Phil. Mag.*, Vol. 16, 1967, p. 1119.
- (18) P. Jung and W. Schilling, *Phys. Rev.*, Vol. 5B, 1972, p. 2046.
- (19) P. Jung, R. L. Chaplin, H. J. Fenzl, K. Reichelt, and P. Wombacher, *Phys. Rev.*, Vol. 8B, 1973, p. 553.

- 57
- (20) M. Biget, P. Vajda, A. Lucasson, and P. Lucasson, *Rad. Effects*, Vol. 21, 1974, p. 229.
 - (21) F. Maury, P. Vajda, M. Biget, A. Lucasson, and P. Lucasson, *Rad. Effects*, Vol. 25, 1975, p. 175.
 - (22) F. Maury, P. Vajda, A. Lucasson and P. Lucasson, *Phys. Rev.*, Vol. 8B, 1973, pp. 5496 and 5506.
 - (23) C. Leimann and G. Leibfried, *Z. Physik*, Vol. 162, 1961, p. 203.
 - (24) W. Bauer and A. Sosin, *J. Appl. Phys.*, Vol. 37, 1966, p. 1780; *ibid* Vol. 37, 1964, p. 703.
 - (25) F. Maury, P. Vajda, A. Lucasson, and P. Lucasson, *Rad. Effects*, Vol. 10, 1971, p. 239.
 - (26) A. B. Pruitt and R. L. Chaplin, *Rad. Effects*, Vol. 10, 1971, p. 235.
 - (27) P. G. Lucasson and R. M. Walker, *Phys. Rev.*, Vol. 127, 1962, p. 485.
 - (28) K. Urban, *Proceedings of the International Conference on Fundamental Aspects of Radiation Damage in Metals*, Gatlinburg, 1975.
 - (29) J. Lindhard, M. Scharff, H. E. Schiøtt, *Mat. Fys. Med. Dan. Vid. Selsk.*, Vol. 33, No. 14, 1963.
 - (30) M. T. Robinson, in Radiation-induced Voids in Metals, J. W. Corbett and L. C. Ianniello, Eds., USAEC Symposium Series, Vol. 26, 1972, p. 397.
 - (31) P. Sigmund, *Rad. Effects*, Vol. 1, 1969, p. 15.
 - (32) M. T. Robinson and I. M. Torrens, *Phys. Rev. B*, Vol. 9, 1974, p. 5008.
 - (33) H. W. Schiøtt, and P. V. Thomsen, *Rad. Effects*, Vol. 14, 1972, p. 39.
 - (34) P. Ehrhart and W. Schilling, *Phys. Rev.*, Vol. B8, 1973, p. 2604.
 - (35) J. Wurm, F. Dworschak, H. Schuster, and H. Wollenberger *Rad. Effects*, Vol. 5, 1970, p. 117.
 - (36) H. H. Andersen and H. Sørensen, *Rad. Effects*, Vol. 14, 1972, p. 49.
 - (37) K. L. Merkle and R. S. Averback, *Proceedings of the International Conference on Fundamental Aspects of Radiation Damage in Metals*, Gatlinburg, 1975.
 - (38) M. Wilkens in Vacancies and Interstitials in Metals, A. Seeger, D. Schumacher, W. Schilling, and J. Diehl, Eds., North-Holland, Amsterdam, 1969, p. 485.
 - (39) M. Rühle, *Radiation Damage in Reactor Materials IAEA*, Vienna, Vol. 1, 1969, p. 113.
 - (40) M. Rühle, in Radiation-induced Voids in Metals, J. W. Corbett and L. C. Ianniello, Eds., USAEC Symposium Series, Vol. 26, 1972, p. 255.
 - (41) A. Seeger, *International Conference Peaceful Uses of Atomic Energy*, Vol. 6, 1958, p. 250.

- (42) L. M. Howe, J. M. McGurn, and R. W. Gilbert, *Acta Met.*, Vol. 14, 1966, p. 801.
- (43) P. Sigmund, G. P. Scheidler, and G. Roth, Proc. Conf. on "Solid State Research with Accelerators," A. N. Goland, Ed., BNL 50083, 1968.
- (44) K. B. Winterbon, P. Sigmund, and J. B. Sanders, *Mat. Fys. Medd. Dan. Vid. Selsk.*, Vol. 37, 1970, p. 14.
- (45) L. E. Thomas, T. Schober, and R. W. Balluffi, *Rad. Effects*, Vol. 1, 1969, p. 257, 269, 279.
- (46) T. Schober, *Phys. Stat. Sol. a*, Vol. 1, 1970, p. 507.
- (47) F. Häussermann, *Phil. Mag.*, Vol. 25, 1972, p. 537.
- (48) K. L. Merkle, Radiation Effects, Ed., Gordon and Breach, 1967, p. 173.
- (49) K. L. Merkle, *Phys. Stat. Sol.*, Vol. 18, 1966, p. 173.
- (50) K. L. Merkle, L. R. Singer, and R. K. Hart, *J. Appl. Phys.*, Vol. 34, 1963, p. 2800.
- (51) K. L. Merkle, *J. Appl. Phys.*, Vol. 38, 1967, p. 301.
- (52) T. S. Noggle and O. S. Oen, *Phys. Rev. Lett.*, Vol. 16, 1966, p. 395.
- (53) J. A. Eades, *Phil. Mag.*, Vol. 19, 1969, p. 47.
- (54) G. Högberg and H. Nordén, *Phys. Stat. Sol. Vol. 33*, K71, 1969.
- (55) K. L. Merkle, L. R. Singer, and J. R. Wrobel, *Appl. Phys. Lett.*, Vol. 17, 1970, p. 6.
- (56) K. L. Merkle and R. L. Lyles, to be published.
- (57) G. D. Doran, *Rad. Effects*, Vol. 2, 1970, p. 249.
- (58) M. M. Wilson, *Phil. Mag.*, Vol. 24, 1971, p. 1023.
- (59) R. V. Hesketh and G. K. Richards, *Proc. Roy. Soc. A*, Vol. 289, 1966, p. 353.
- (60) M. O. Ruault, B. Jouffrey, and P. Joyes, *Phil. Mag.*, Vol. 25, 1972, p. 833.
- (61) E. Johnson and J. A. Ytterhus, *Phil. Mag.*, Vol. 28, 1973, p. 489.
- (62) D. I. R. Norris, *Phil. Mag.*, Vol. 19, 1969, p. 527.
- (63) C. Gomez-Giraldez, B. Hertel, M. Rühle, and M. Wilkens Application of Ion Beams to Metals, p. 469.
- (64) F. Häussermann, *Phil. Mag.*, Vol. 25, 1972, p. 561; *ibid.* Vol. 25, 1972, p. 583.
- (65) B. C. Masters, *Phil. Mag.*, Vol. 11, 1965, p. 881.
- (66) J. T. Buswell, *Phil. Mag.*, Vol. 22, 1970, p. 787.
- (67) C. A. English, B. L. Eyre, J. Summers, and H. Wadley, Proceedings of the International Conference on Fundamental Aspects of Radiation Damage in Metals, Gatlinburg, 1975.
- (68) C. A. English, B. L. Eyre, H. Wadley, and A. Y. Statopoulos, Proceedings of the International Conference on Fundamental Aspects of Radiation Damage in Metals, Gatlinburg, 1975.
- (69) K. L. Merkle, Radiation Damage in Reactor Materials, Vol. 1, IAEA, Vienna, 1969, p. 159.

- 56
- (70) P. P. Pronko and K. L. Merkle, Applications of Ion Beams to Metals, S. T. Picraux, E. P. EerNisse, and F. L. Vook, Eds., Plenum Press, 1974, p. 481.
 - (71) K. L. Merkle, in Physics of Ionized Gases 1974, V. Vujnovic, Ed., University of Zagreb, 1975, p. 505.
 - (72) R. L. Lyles and K. L. Merkle, in Proceedings of International Conference on Radiation Effects and Tritium Technology for Fusion Reactors, Gatlinburg, 1975.
 - (73) J. R. Beeler, J. Nucl. Mater., Vol. 53, 1974, p. 207 and M. T. Robinson, private communication.
 - (74) J. R. Beeler, Phys. Rev., Vol. 150, 1966, p. 470.
 - (75) M. L. Jenkins, K.-H. Katerbau, and M. Wilkens, Proceedings of the International Conference on Fundamental Aspects of Radiation Damage in Metals, Gatlinburg, 1975.
 - (76) P. B. Hirsch et al., Electron Microscopy of Thin Crystals, London, Butterworths, 1965.
 - (77) M. Wilkens, M. Rühle, and F. Häussermann, J. Microscopie, Vol. 16, 1973, p. 199.
 - (78) M. Wilkens, in Modern Diffraction and Imaging Techniques in Materials Science, North-Holland, 1970, p. 233.
 - (79) M. Rühle, M. Wilkens, and V. Essmann, Phys. Stat. Sol. Vol. 11, 1965, p. 819.
 - (80) M. M. Wilson, Rad. Effects, Vol. 1, 1969, p. 207.
 - (81) M. M. Wilson and P. B. Hirsch, Phil. Mag., Vol. 25, 1972, p. 983.
 - (82) M. O. Ruault, B. Jouffrey, J. Chaumont, and H. Bernas, in Applications of Ion Beams to Metals, Plenum Press, 1974, p. 459.
 - (83) J. B. Mitchell and W. L. Bell, to be published in Acta Met., 1975.
 - (84) M. Wilkens and M. Rühle, Phys. Stat. Sol. b, Vol. 49, 1972, p. 749.
 - (85) K. L. Merkle, to be published.
 - (86) M. Jenkins, private communication.
 - (87) J. L. Whitton, Canad. J. Phys. Vol. 45, 1967, p. 1947.
 - (88) D. I. R. Norris, Phil. Mag., Vol. 19, 1969, p. 653.
 - (89) H. H. Andersen and P. Sigmund, Nucl. Instr. Methods, Vol. 38, 1965, p. 238.
 - (90) M. A. Kumakhov, Phys. Stat. Sol., Vol. 30, 1968, p. 379
 - (91) T. S. Noggle and J. H. Barrett, Phys. Stat. Sol., Vol. 36, 1969, p. 761.
 - (92) T. Schober and R. W. Balluffi, Can. J. Phys. Vol. 47, 1969, p. 1221.
 - (93) T. Schober and R. W. Balluffi, Phys. Stat. Sol., Vol. 27, 1969, p. 195.
 - (94) K. L. Merkle, Proceedings of the 26th Annual EMSA Meeting, 1969, p. 278.
 - (95) J. Silcox and P. B. Hirsch, Phil. Mag., Vol. 4, 1959, p. 1356.

- (96) M. J. Makin, A. D. Whapham, and F. J. Minter, *Phil. Mag.* Vol. 7, 1962, p. 285.
- (97) M. Rühle, *Phys. Stat. Sol.*, Vol. 19, 1967, pp. 263 and 279.
- (98) K. G. McIntyre, *Phil. Mag.*, Vol. 15, 1967, p. 205.
- (99) M. Rühle and J. C. Crump, *Phys. Stat. Sol. a*, Vol. 2, 1970, p. 257.
- (100) M. Ipohorsky and L. M. Brown, *Phil. Mag.*, Vol. 22, 1970, p. 931.
- (101) M. Rühle, F. Häussermann, and M. Rapp, *Phys. Stat. Sol.*, Vol. 39, 1970, pp. 609 and 621.
- (102) A. Bourret and D. Dautreppe, *Phys. Stat. Sol.*, Vol. 29, 1968, p. 283.
- (103) R. P. Tucker and S. M. Ohr, *Phil. Mag.*, Vol. 16, 1967, p. 643.
- (104) B. A. Loomis and S. B. Gerber, *Acta Met.*, Vol. 21, 1973, p. 165.
- (105) J. B. Mitchell, R. A. Van Konynenburg, M. W. Guinan, and C. J. Echer, *Phil. Mag.*, Vol. 31, 1975, p. 919.
- (106) K. L. Merkle, *Nucl. Tech.*, Vol. 22, 1974, p. 66.
- (107) The 14-MeV neutron Au recoil spectrum has been calculated by C. M. Logan, Lawrence Livermore Laboratory.